

# Thermal structure of oceanic transform faults

Mark D. Behn\*

Margaret S. Boettcher†

Greg Hirth

Department of Geology and Geophysics, Woods Hole Oceanographic Institution,  
Woods Hole, Massachusetts 02543, US

## ABSTRACT

**We use three-dimensional finite element simulations to investigate the temperature structure beneath oceanic transform faults. We show that using a rheology that incorporates brittle weakening of the lithosphere generates a region of enhanced mantle upwelling and elevated temperatures along the transform; the warmest temperatures and thinnest lithosphere are predicted to be near the center of the transform. Previous studies predicted that the mantle beneath oceanic transform faults is anomalously cold relative to adjacent intraplate regions, with the thickest lithosphere located at the center of the transform. These earlier studies used simplified rheologic laws to simulate the behavior of the lithosphere and underlying asthenosphere. We show that the warmer thermal structure predicted by our calculations is directly attributed to the inclusion of a more realistic brittle rheology. This temperature structure is consistent with a wide range of observations from ridge-transform environments, including the depth of seismicity, geochemical anomalies along adjacent ridge segments, and the tendency for long transforms to break into small intratransform spreading centers during changes in plate motion.**

**Keywords:** oceanic transform faults, mid-ocean ridges, fault rheology, intratransform spreading centers.

## INTRODUCTION

Oceanic transform faults are ideal for studying the behavior of strike-slip faults because of the relatively simple thermal and kinematic structure and composition of the oceanic lithosphere. On continents, fault rheology is influenced by mantle thermal structure, variations in crustal thickness, and heterogeneous lithology. By contrast, the rheology of the oceanic upper mantle is primarily controlled by temperature. In the ocean basins, the maximum depth of intraplate earthquakes (Chen and Molnar, 1983; McKenzie et al., 2005) correlates with the location of the 600 °C isotherm calculated from a half-space cooling model. Similarly, the maximum depth of transform fault earthquakes corresponds to the location of the 600 °C isotherm derived by averaging the half-space thermal structures on either side of the fault (Abercrombie and Ekström, 2001). Extrapolation of laboratory data on olivine also indicates that the transition from stable to unstable frictional sliding occurs at ~600 °C at geologic strain rates (Boettcher et al., 2007). Furthermore, microstructures in peridotite mylonites from oceanic transforms show that localized viscous deformation occurs at 600–800 °C (e.g., Jaroslow et al., 1996; Warren and Hirth, 2006).

While a half-space cooling model successfully predicts the maximum depth of transform earthquakes, it neglects many physical processes that occur in the crust and upper mantle (e.g., advective heat transport resulting from temperature-dependent viscous flow, hydrothermal circulation, and viscous dissipation). Numerical models that incorporate three-dimensional (3-D) advective and conductive heat transport indicate that the mantle beneath oceanic transform faults is anomalously cold relative to a half-space model (Furlong et al., 2001; Phipps Morgan and Forsyth, 1988; Shen and Forsyth, 1992). Lower temperatures result from conductive cooling from the adjacent old lithosphere across the transform, and decreased mantle upwelling beneath the transform. These effects result in an increase of as

much as ~75% in lithospheric thickness beneath the center of a transform fault relative to a half-space cooling model, as well as significant cooling of the mantle beneath the ends of the adjacent spreading centers. This characteristic ridge-transform thermal structure is invoked to explain the focusing of crustal production toward the centers of ridge segments (e.g., Magde and Sparks, 1997), geochemical evidence for colder upper mantle near segment ends (e.g., Niu and Batiza, 1994), and increased normal fault displacement near segment ends (Shaw and Lin, 1993). However, correlating the maximum depth of earthquakes on transform faults with this colder thermal structure implies that the transition from stable to unstable frictional sliding occurs at ~350 °C, which is inconsistent with both laboratory studies and the depth of intraplate earthquakes.

To address the discrepancies between the geophysical observations and predictions of previous modeling studies, we investigate the importance of fault rheology on the thermo-mechanical behavior of oceanic transform faults. Earlier studies used simplified rheologic laws to simulate the behavior of the lithosphere and underlying asthenosphere. We show that brittle weakening of the lithosphere strongly reduces the effective viscosity beneath the transform, resulting in enhanced upwelling and thinning of the lithosphere. Our calculations suggest that the thermal structure of oceanic transform faults is similar to that predicted from half-space cooling, but with the warmest temperatures located near the center of the transform. These results have implications for the mechanical behavior of oceanic transforms, melt generation and migration at mid-ocean ridges, and the long-term response of transform faults to changes in plate motion.

## MODEL SETUP

To solve for coupled 3-D steady-state incompressible mantle flow and thermal structure, we use the COMSOL 3.2 finite element software package (for details, see GSA Data Repository<sup>1</sup>). In all simulations, flow is driven by imposing horizontal velocities parallel to a 150 km transform fault along the top boundaries of the model space, assuming full spreading rates ranging from 3 to 12 cm/yr (Fig. 1). The base of the model is stress free, and thus open to convective flux without resistance from the underlying mantle. Symmetric boundary conditions are imposed on the sides of the model space parallel to the spreading direction, and the boundaries perpendicular to spreading are open to convective flux. The temperature,  $T$ , across the top and bottom of the model space is set to  $T_s = 0$  °C and  $T_m = 1300$  °C, respectively ( $T_s$ —temperature at the surface;  $T_m$ —temperature of the mantle). Flow associated with buoyancy caused by variations in temperature and composition is ignored.

To investigate the importance of rheology on thermal structure, we examined four scenarios with increasingly realistic descriptions of mantle rheology: (1) constant viscosity, (2) temperature-dependent viscosity, (3) temperature-dependent viscosity with a predefined weak zone around the transform, and (4) temperature-dependent viscosity with a visco-plastic approximation for brittle weakening. For simplicity, and comparison with previous studies, we ignore the effects of viscous dissipation. In all models we assume a Newtonian mantle rheology. In models 2–4 the temperature dependence of viscosity is calculated by:

<sup>1</sup>GSA Data Repository item 2007076, description of the numerical model and sensitivity tests for model parameters used in this study, is available online at [www.geosociety.org/pubs/ft2007.htm](http://www.geosociety.org/pubs/ft2007.htm), or on request from [editing@geosociety.org](mailto:editing@geosociety.org) or Documents Secretary, GSA, P.O. Box 9140, Boulder, CO 80301, USA.

\*E-mail: [mbehn@whoi.edu](mailto:mbehn@whoi.edu).

†Current address: U.S. Geological Survey, Menlo Park, California 94025, USA.

$$\eta = \eta_0 \exp \left[ \frac{Q_0}{R} \left( \frac{1}{T} - \frac{1}{T_m} \right) \right], \quad (1)$$

where  $\eta_0$  is the reference viscosity of  $10^{19}$  Pa·s,  $Q_0$  is the activation energy, and  $R$  is the gas constant. We use an activation energy of 250 kJ/mol. This value represents a reduction of a factor of two relative to the laboratory value as a linear approximation for nonlinear rheology (Christensen, 1983). Viscosity is not allowed to exceed  $10^{23}$  Pa·s.

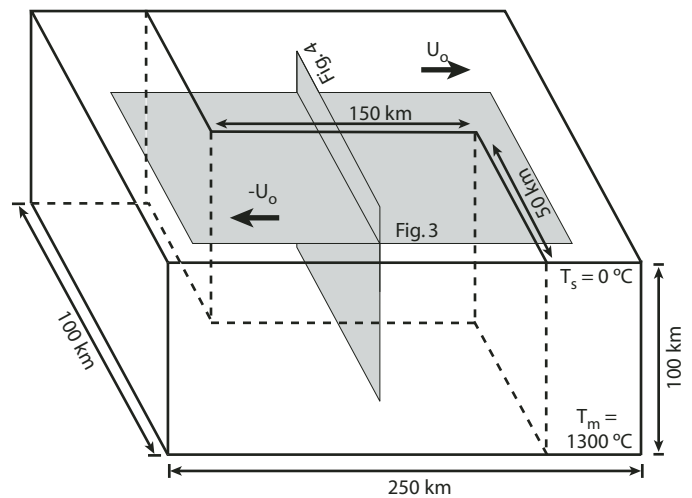
### INFLUENCE OF 3-D MANTLE FLOW ON TRANSFORM THERMAL STRUCTURE

Figure 2 illustrates the thermal structure calculated at the center of the transform fault from models 1–4, as well as that determined by averaging half-spacing cooling models on either side of the transform. Because the thermal structure calculated from half-space cooling is equal on the adjacent plates, the averaging approach predicts the same temperature at the center of the transform fault as for the adjacent intraplate regions. We use the half-space model as a reference for evaluating whether our 3-D calculations predict relative cooling or heating below the transform. The solution for a constant viscosity mantle (model 1) was determined by Phipps Morgan and Forsyth (1988); our results agree with theirs to within 5% throughout the model space. This solution predicts significantly colder temperatures at the center of the transform than does half-space cooling, with the depth of the 600 °C isotherm increasing from ~7 km for the half-space model to ~12 km for the constant viscosity solution (Fig. 2A). Phipps Morgan and Forsyth (1988) noted that this reduction in temperature results from decreased mantle upwelling beneath the transform relative to enhanced upwelling under the ridge axis. Shen and Forsyth (1992) showed that incorporating temperature-dependent viscosity (e.g., model 2) produces enhanced upwelling and warmer temperatures beneath the ridge axis relative to a constant viscosity mantle (Fig. 3). However, away from the ridge axis, the two solutions are similar and result in almost identical temperature-depth profiles at the center of the transform (Figs. 2A and 3).

### INFLUENCE OF FAULT ZONE RHEOLOGY ON TRANSFORM THERMAL STRUCTURE

Several observations indicate that oceanic transform faults are weaker than the surrounding lithosphere. Comparisons of abyssal hill fabric near transforms to predictions of fault patterns from modeling suggest that mechanical coupling across the fault is weak on geologic time scales (Behn et al., 2002). Furthermore, serpentinized peridotites are frequently dredged in transform valleys and valley walls (Cannat et al., 1991; Dick et al., 1991), which may promote frictional weakening (Escartín et al., 2001; Rutter and Brodie, 1987). In comparison to continental strike-slip faults, oceanic transforms have high seismic deficits (Boettcher and Jordan, 2004), suggesting that ocean transforms accommodate large amounts of aseismic slip.

In model 3 we simulate the effect of a weak fault zone by setting the viscosity to  $10^{19}$  Pa·s in a 5-km-wide region surrounding the transform that extends to a depth of 20 km. This narrow fault zone has a viscosity 3–4 orders of magnitude lower than the surrounding regions. This approach is similar to that used by Furlong et al. (2001) and van Wijk and Blackman (2005), although these earlier studies modeled deformation in a visco-elastic system in which the transform fault was simulated as a shear stress-free plane. Our models show that incorporating the weak fault zone of finite width produces slightly warmer conditions along the transform than for either a constant viscosity mantle (model 1) or temperature-dependent viscosity without an imposed fault zone (model 2). However, the predicted temperatures from the fault zone model remain colder than those calculated by the half-space cooling model (Figs. 2A and 3). Varying the maximum depth of the weak zone from 5 km to the base of the model space does not significantly influence the thermal structure.



**Figure 1. Model setup for numerical simulations of mantle flow and thermal structure at oceanic transform faults. All calculations are performed for 150-km-long transform. Model space is 100 km deep and is sufficient to resolve thermal structure for spreading rates considered in this study. Finite element grid spacing decreases toward transform and ridge axes, reaching minimum value of 3.75 km. Locations of cross sections used in Figures 2–4 are shown in gray.**

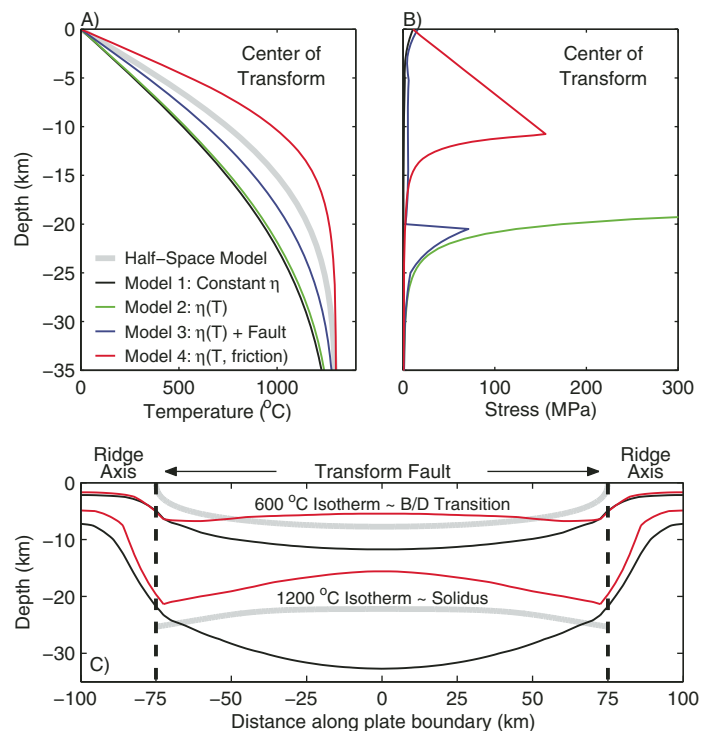


**Figure 2. Thermal structure (A) and stress (B) calculated vs. depth at center of 150-km-long transform fault assuming full spreading rate of 6 cm/yr. C: Location of 600 °C and 1200 °C isotherms along plate boundary for half-space model (gray), model 1 (black), and model 4 (red). B/D—Brittle/Ductile.**

Representing the transform as a predefined zone of uniform weakness clearly oversimplifies the brittle processes occurring within the lithosphere. In model 4, we incorporate a more realistic formulation for fault zone behavior by using a visco-plastic rheology to simulate brittle weakening (Chen and Morgan, 1990). Brittle strength is approximated by a friction law:

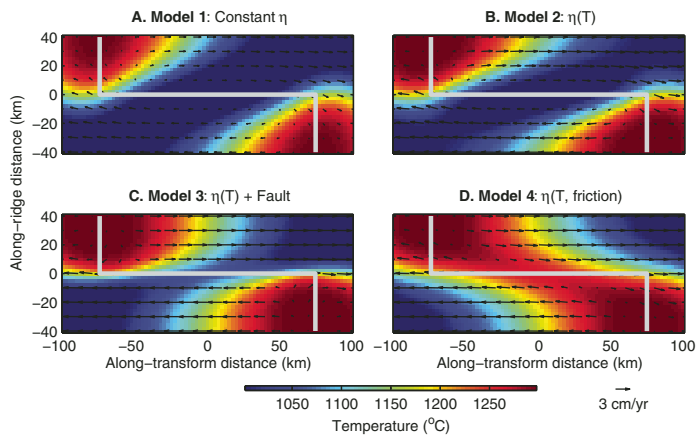


**Figure 3.** Cross sections of mantle temperature at depth of 20 km and full spreading rate of 6 cm/yr. **A:** Model 1: constant viscosity of  $10^{19}$  Pa·s. **B:** Model 2: temperature-dependent viscosity. **C:** Model 3: temperature-dependent viscosity with weak fault zone. **D:** Model 4: temperature-dependent viscosity with frictional failure law. Black arrows indicate horizontal flow velocities (note that finite element grid spacing is significantly finer than spacing of flow vectors). Gray lines show position of plate boundary. Location of horizontal cross section is indicated in Figure 1. Note that model 4 incorporating frictional resistance predicts significantly warmer temperatures along transform than models 1–3.

$$\tau_{\max} = C_0 + \mu \rho g z, \quad (2)$$

in which  $C_0$  is cohesion (10 MPa),  $\mu$  is the friction coefficient (0.6),  $\rho$  is density ( $3300 \text{ kg/m}^3$ ),  $g$  is gravitational acceleration, and  $z$  is depth. Following Chen and Morgan (1990), the maximum effective viscosity is then limited by:

$$\eta = \frac{\tau_{\max}}{\sqrt{2\dot{\epsilon}_{II}}}, \quad (3)$$

where  $\dot{\epsilon}_{II}$  is the second invariant of the strain-rate tensor. This brittle failure law limits viscosity near the surface, where the temperature dependence of equation 1 produces unrealistically high viscosities and stresses (Fig. 2B).

The inclusion of the visco-plastic rheology results in significantly higher temperatures beneath the transform than predicted by models 1–3 or half-space cooling (Figs. 2A and 3). These higher temperatures are a direct result of brittle weakening of the lithosphere, which reduces the effective viscosity as much as 2 orders of magnitude in a 10-km-wide region surrounding the fault zone. Unlike model 3, the width of this region is not predefined and develops as a function of the rheology and boundary conditions. The zone of decreased viscosity enhances passive upwelling beneath the transform (relative to model 2), which in turn increases upward heat transport, warming the fault zone and further reducing viscosity (Fig. 4). The result is a characteristic thermal structure in which the transform fault is warmest at its center and cools toward the adjacent ridge segments (Fig. 2C). Moreover, the center of the transform is warmer than adjacent lithosphere of the same age. Sensitivity tests show that for a realistic range of rheologic parameters (e.g.,  $C_0$ ,  $\mu$ , and  $Q$ ) there is little influence on the resulting thermal structure (Fig. DR2; see footnote 1), implying that it is the process of brittle weakening, not the specific model parameters, that generates the warmer temperatures along the transform. Although we have neglected the effects of shear heating, inclusion of this process will only act to further increase temperatures along the transform. As shown in Figure DR3 [see footnote 1], the relative heating resulting from the inclusion of a visco-plastic rheology is apparent for a wide range of spreading rates.

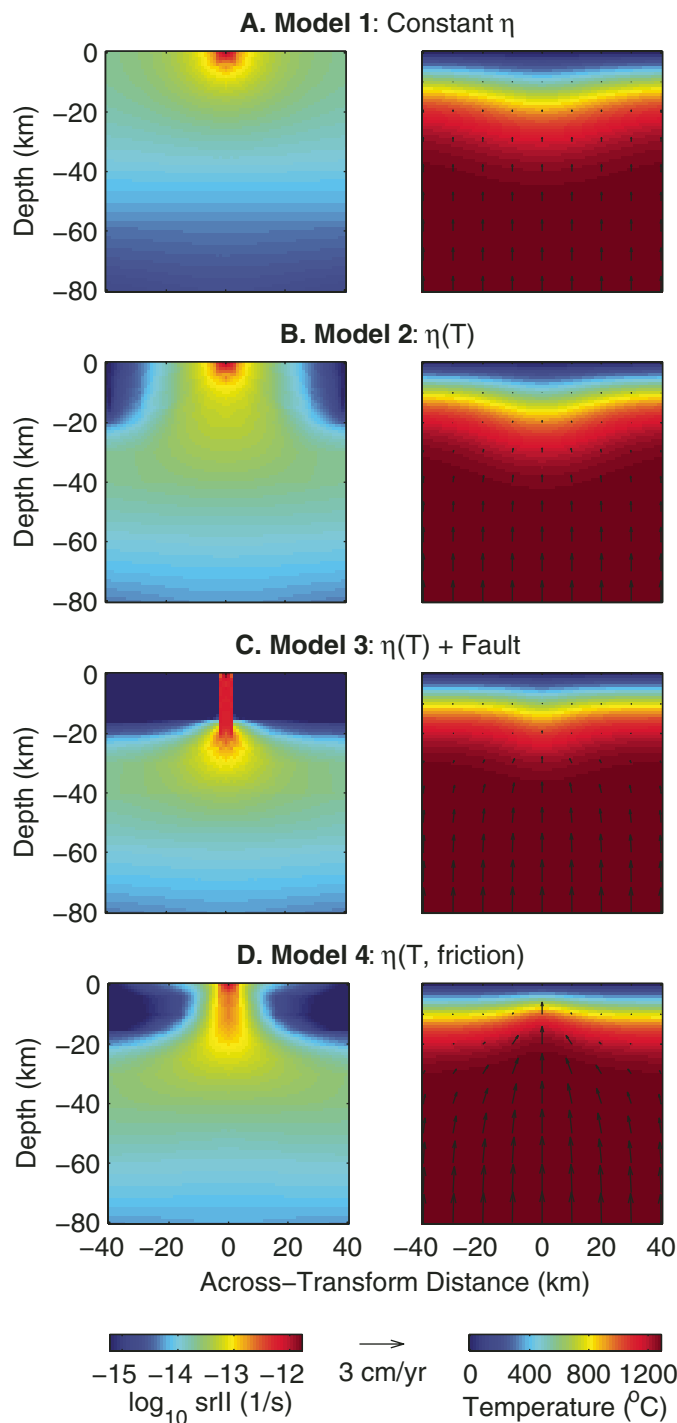


**Figure 4.** Vertical cross sections through center of transform fault showing (left) strain rate, and (right) temperature and mantle flow for models 1–4 at full spreading rate of 6 cm/yr. Locations of cross sections are indicated in Figure 1. Note that enhanced upwelling below the transform results in a warmer thermal structure for model 4 compared to models 1–3.

## IMPLICATIONS FOR THE BEHAVIOR OF OCEANIC TRANSFORM FAULTS

Our numerical simulations indicate that brittle weakening plays an important role in controlling the thermal structure beneath oceanic transform faults. Specifically, incorporating a more realistic treatment of brittle rheology results in a temperature structure that is consistent with the geo-

physical and geochemical observations from ridge-transform environments. The temperatures below the transform predicted in model 4 are similar to a half-space cooling model. This indicates that the maximum depth of transform fault seismicity is limited by the ~600 °C isotherm, consistent with the seismological and microstructural studies described in the Introduction.

While the inclusion of a visco-plastic rheology results in significant warming beneath the transform fault, the temperatures at the ends of the adjacent ridge segments change only slightly relative to the solution for a constant viscosity mantle. In particular, both models predict a region of cooling along the adjacent ridge segments that extends 15–20 km from the transform fault (Fig. 2C). Thus, model 4 is consistent with the transform edge effect that is frequently invoked to explain geophysical and geochemical variations along ridge axes outlined in the Introduction.

Elevated temperatures near the center of the transform may also promote the development of intratransform spreading centers during changes in plate motion (Lonsdale, 1989; Menard and Atwater, 1969). This leaky transform phenomenon is attributed to the weakness of oceanic transform faults relative to the surrounding lithosphere (e.g., Searle, 1983). However, the leaky transform hypothesis conflicts with the thermal structure predicted from models 1–3, which show the transform to be a region of anomalously cold, thick lithosphere. In contrast, the thermal structure predicted by model 4 indicates that transforms are hottest and weakest near their centers (Fig. 2C). Higher temperatures near the center of the transform faults would enhance melting and promote the migration of off-axis melts into the transform zone, further weakening the plate boundary. Thus, perturbations in plate motion, which generate extension across the transform, are likely to result in rifting and additional melting in these regions.

The incorporation of the brittle rheology also promotes strain localization on the plate scale. If transforms were regions of thick, cold lithosphere (as predicted by models 1–3), then over time deformation would tend to migrate outward from the transform zone into the adjacent regions of thinner lithosphere. In contrast, the warmer thermal structure that results from the incorporation of a visco-plastic rheology will keep deformation localized within the transform zone on time scales corresponding to the age of ocean basins.

In summary, brittle weakening of the lithosphere along oceanic transform faults generates a region of enhanced mantle upwelling and elevated temperatures relative to adjacent intraplate regions. The thermal structure is similar to that predicted by a half-space cooling model, but with the warmest temperatures located at the center of the transform. This characteristic upper mantle temperature structure is consistent with a wide range of geophysical and geochemical observations, and provides important constraints on the future interpretation of microseismicity, heat flow, and basalt and peridotite geochemistry in ridge-transform environments.

#### ACKNOWLEDGMENTS

We thank J. McGuire, L. Montési, P. Gregg, J. Lin, H. Dick, and D. Forsyth for discussions that helped motivate this work. We also appreciate thoughtful reviews from D. Blackman and S. Sobolev. Funding was provided by National Science Foundation grants EAR-0405709, EAR-0509882, OCE-0548672, and OCE-0623188.

#### REFERENCES CITED

Abercrombie, R.E., and Ekström, G., 2001, Earthquake slip on oceanic transform faults: *Nature*, v. 410, p. 74–77, doi: 10.1038/35065064.  
 Behn, M.D., Lin, J., and Zuber, M.T., 2002, Evidence for weak oceanic transform faults: *Geophysical Research Letters*, v. 29, 2207, doi: 10.1029/2002GL015612.  
 Boettcher, M.S., and Jordan, T.H., 2004, Earthquake scaling relations for mid-ocean ridge transform faults: *Journal of Geophysical Research*, v. 109, B12302, doi: 10.1029/2004JB003110.

Boettcher, M.S., Hirth, G., and Evans, B., 2007, Olivine friction at the base of the oceanic seismogenic zones: *Journal of Geophysical Research*, v. 112, B01205, doi: 10.1029/2006JB004301.  
 Cannat, M., Mamaloukas-Frangoulis, V., Auzende, J.-M., Bideau, D., Bonatti, E., Honnorez, J., Lagabrielle, Y., Malavielle, J., and Mevel, C., 1991, A geological cross-section of the Vema fracture zone transverse ridge: *Atlantic Ocean: Journal of Geodynamics*, v. 13, p. 97–118, doi: 10.1016/0264-3707(91)90034-C.  
 Chen, W.-P., and Molnar, P., 1983, Focal depths of intracontinental and intraplate earthquakes and their implications for the thermal and mechanical properties of the lithosphere: *Journal of Geophysical Research*, v. 88, p. 4183–4214.  
 Chen, Y., and Morgan, W.J., 1990, A nonlinear rheology model for mid-ocean ridge axis topography: *Journal of Geophysical Research*, v. 95, p. 17,583–17,604.  
 Christensen, U., 1983, Convection in a variable-viscosity fluid: Newtonian versus power-law rheology: *Earth and Planetary Science Letters*, v. 64, p. 153–162, doi: 10.1016/0012-821X(83)90060-2.  
 Dick, H.J.B., Schouten, H., Meyer, P.S., Gallo, D.G., Bergh, H., Tyce, R., Patriat, P., Johnson, K.T.M., Snow, J., and Fisher, A., 1991, Tectonic evolution of the Atlantis II Fracture Zone, in Von Herzen, R.P., and Robinson, P.T., *Proceedings of the Ocean Drilling Program, Scientific results, Volume 118: College Station, Texas, Ocean Drilling Program*, p. 359–398.  
 Escartín, J., Hirth, G., and Evans, B., 2001, Strength of slightly serpentinized peridotites: Implications for the tectonics of oceanic lithosphere: *Geology*, v. 29, p. 1023–1026, doi: 10.1130/0091-7613(2001)029<1023:SOSSPI>2.0.CO;2.  
 Furlong, K.P., Sheaffer, S.D., and Malservisi, R., 2001, Thermal-rheological controls on deformation within oceanic transforms, in Holdsworth, R.E., et al., eds., *The nature and tectonic significance of fault zone weakening: Geological Society [London] Special Publication 186*, p. 65–84.  
 Jaroslaw, G.E., Hirth, G., and Dick, H.J.B., 1996, Abyssal peridotite mylonites: Implications for grain-size sensitive flow and strain localization in the oceanic lithosphere: *Tectonophysics*, v. 256, p. 17–37, doi: 10.1016/0040-1951(95)00163-8.  
 Lonsdale, P., 1989, Segmentation of the Pacific-Nazca spreading center, 1°N–20°S: *Journal of Geophysical Research*, v. 94, p. 12,197–12,225.  
 Magde, L.S., and Sparks, D.W., 1997, Three-dimensional mantle upwelling, melt generation, and melt migration beneath segment slow spreading ridges: *Journal of Geophysical Research*, v. 102, p. 20,571–20,583, doi: 10.1029/97JB01278.  
 McKenzie, D., Jackson, J., and Priestley, K., 2005, Thermal structure of oceanic and continental lithosphere: *Earth and Planetary Science Letters*, v. 233, p. 337–349, doi: 10.1016/j.epsl.2005.02.005.  
 Menard, H.W., and Atwater, T., 1969, Origin of fracture zone topography: *Nature*, v. 222, p. 1037–1040, doi: 10.1038/2221037a0.  
 Niu, Y., and Batiza, R., 1994, Magmatic processes at a slow spreading ridge segment: 26°S Mid-Atlantic Ridge: *Journal of Geophysical Research*, v. 99, p. 19,719–19,740, doi: 10.1029/94JB01663.  
 Phipps Morgan, J., and Forsyth, D.W., 1988, Three-dimensional flow and temperature perturbations due to a transform offset: Effects on oceanic crust and upper mantle structure: *Journal of Geophysical Research*, v. 93, p. 2955–2966.  
 Rutter, E.H., and Brodie, K.H., 1987, On the mechanical properties of oceanic transform faults: *Annales Tectonicae*, v. 1, p. 87–96.  
 Searle, R.C., 1983, Multiple, closely spaced transform faults in fast-slipping fracture zones: *Geology*, v. 11, p. 607–611, doi: 10.1130/0091-7613(1983)11<607:MCSTFI>2.0.CO;2.  
 Shaw, P.R., and Lin, J., 1993, Causes and consequences of variations in faulting style at the Mid-Atlantic Ridge: *Journal of Geophysical Research*, v. 98, p. 21,839–21,851.  
 Shen, Y., and Forsyth, D.W., 1992, The effects of temperature- and pressure-dependent viscosity on three-dimensional passive flow of the mantle beneath a ridge-transform system: *Journal of Geophysical Research*, v. 97, p. 19,717–19,728.  
 van Wijk, J.W., and Blackman, D.K., 2005, Deformation of oceanic lithosphere near slow-spreading ridge discontinuities: *Tectonophysics*, v. 407, p. 211–225, doi: 10.1016/j.tecto.2005.08.009.  
 Warren, J.M., and Hirth, G., 2006, Grain size sensitive deformation mechanisms in naturally deformed peridotites: *Earth and Planetary Science Letters*, v. 248, p. 438–450.

Manuscript received 28 June 2006

Revised manuscript received 26 October 2006

Manuscript accepted 29 October 2006

Printed in USA

1 **GSA Online Data Repository**  
 2 **Supplement to “On the thermal structure of oceanic transform faults”**  
 3 **Mark D. Behn, Margaret S. Boettcher, and Greg Hirth**

4  
 5 **1. Finite Element Methods**

6 We use COMSOL Multiphysics 3.2 to solve for the steady-state conservation of mass

$$7 \quad \nabla \cdot \mathbf{u} = 0 \quad (1)$$

8 momentum

$$9 \quad -\eta \nabla^2 \mathbf{u} + \rho(\mathbf{u} \cdot \nabla) \mathbf{u} + \nabla p = \rho \mathbf{g} \quad (2)$$

10 and energy

$$11 \quad \nabla \cdot (-k \nabla T) = -\rho C_p \mathbf{u} \cdot \nabla T + Q \quad (3)$$

12 in an incompressible viscous fluid. Here  $\mathbf{u}$  is velocity,  $\eta$  is viscosity,  $\rho$  is density,  $p$  is  
 13 pressure,  $\mathbf{g}$  is gravity,  $k$  is thermal conductivity,  $T$  is temperature,  $C_p$  is specific heat, and  
 14  $Q$  is a heat source term. (Bold symbols indicate vector quantities). Because we ignore all  
 15 heat sources, including viscous dissipation (i.e., frictional heating),  $Q = 0$  in all our  
 16 simulations.

17 **2. Numerical Resolution and Sensitivity Tests**

18 To insure that our numerical results are not the artifact of the numerical parameters  
 19 chosen in this study we have performed a series of resolution and sensitivity tests. Figure  
 20 S1 illustrates a grid resolution test showing the grid spacing used in this study is  
 21 sufficient to resolve the zone of plastic deformation along the fault. Furthermore, the  
 22 depth of the model space (100 km) is large enough such that the stress and temperature  
 23 condition at the base of the model space do not influence the temperatures along the  
 24 transform.

25 We also test the sensitivity of our results to variations in the coefficient of friction and  
 26 cohesive strength (Figures S2A & S2B) and changes in activation energy for viscous  
 27 deformation (Figures S2C & S2D). We find that variations in friction parameters have  
 28 only a small effect of the temperature structure beneath the transform. The activation  
 29 energy has a somewhat larger effect, however even with extremely low values (e.g., 75  
 30 kJ/mol) the temperature at the center of the transform remains warmer than predicted by  
 31 the averaged half-space model.

32        Although we have not explicitly modeled the effects of non-linear rheology, several  
33 previous studies have examined the importance of a non-linear viscosity law on mantle  
34 flow and thermal structure in a segmented ridge-transform system (Furlong et al., 2001;  
35 Shen and Forsyth, 1992; van Wijk and Blackman, 2004). Without the effects of brittle  
36 weakening, these earlier studies predicted temperatures below the transform that were  
37 significantly colder than a half-space cooling model. Thus, we conclude that the  
38 inclusion of a visco-plastic rheology is the key factor for producing the warmer transform  
39 fault thermal structure.

40        To determine whether the transform temperature structure is sensitive to spreading  
41 rate we compare Model 1 and Model 4 to the averaged half-space cooling model over a  
42 range of spreading rates (Figure S3). These results indicate that the relative heating  
43 effect associated with adding the visco-plastic rheology (Model 4) is apparent over the  
44 range of spreading typical of fast- to slow-spreading mid-ocean ridges.

45

46

46 **Figure Captions:**

47 **Figure S1:** Depth of the 600°C isotherm at the center of the transform as a function of  
48 the across-transform grid spacing for a 100 km deep model space (blue circles). As grid  
49 spacing decrease there is a modest change in the depth to the 600°C isotherm, with  
50 convergence for grid spacings  $\leq 5$  km. Red triangle and black square show results for  
51 models with deeper box sizes of 125 km and 150 km, respectively.

52 **Figure S2:** Sensitivity tests of temperature and stress at the center of the transform fault  
53 to as a function of the rheologic parameters. A&B show temperature and stress state,  
54 respectively, for varying coefficient of friction ( $\mu$ ) and cohesive strength ( $C_0$ ). C&D  
55 illustrate the effects of varying the activation energy for viscous deformation ( $Q$ ).

56 **Figure S3:** Depth to the 600°C isotherm at the center of the transform fault as a function  
57 of full spreading rate. Solutions are shown for Model 1 (constant viscosity, open squares)  
58 and Model 4 (temperature-dependent visco-plastic rheology, filled circles), and the  
59 averaged half-space solution (grey line).

60

61 **References:**

- 62 Furlong, K.P., Sheaffer, S.D., and Malservisi, R., 2001, Thermal-rheological controls on  
63 deformation within oceanic transforms, *in* Holdsworth, R.E., Strachan, R.A.,  
64 Magloughlin, J.F., and Knipe, R.J., eds., *The Nature and Tectonic Significance of*  
65 *Fault Zone Weakening*, Volume 186: London, Geology Society, p. 65-84.  
66 Shen, Y., and Forsyth, D.W., 1992, The effects of temperature- and pressure-dependent  
67 viscosity on three-dimensional passive flow of the mantle beneath a ridge-  
68 transform system: *J. Geophys. Res.*, v. 97, p. 19,717-19,728.  
69 van Wijk, J.W., and Blackman, D.K., 2004, Deformation of oceanic lithosphere near  
70 slow-spreading ridge discontinuities: *Tectonophys.*, v. 407, p. 211-225.  
71  
72

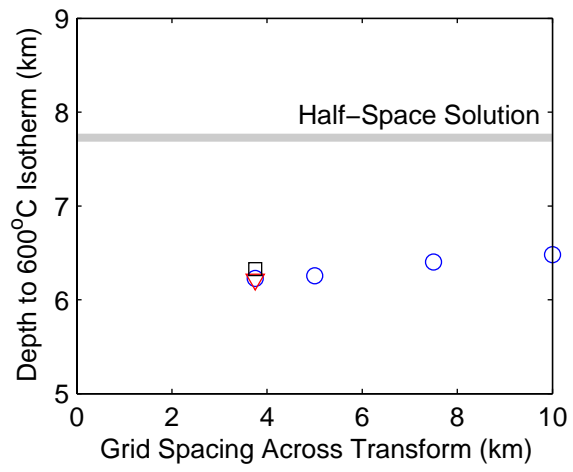


Figure S1

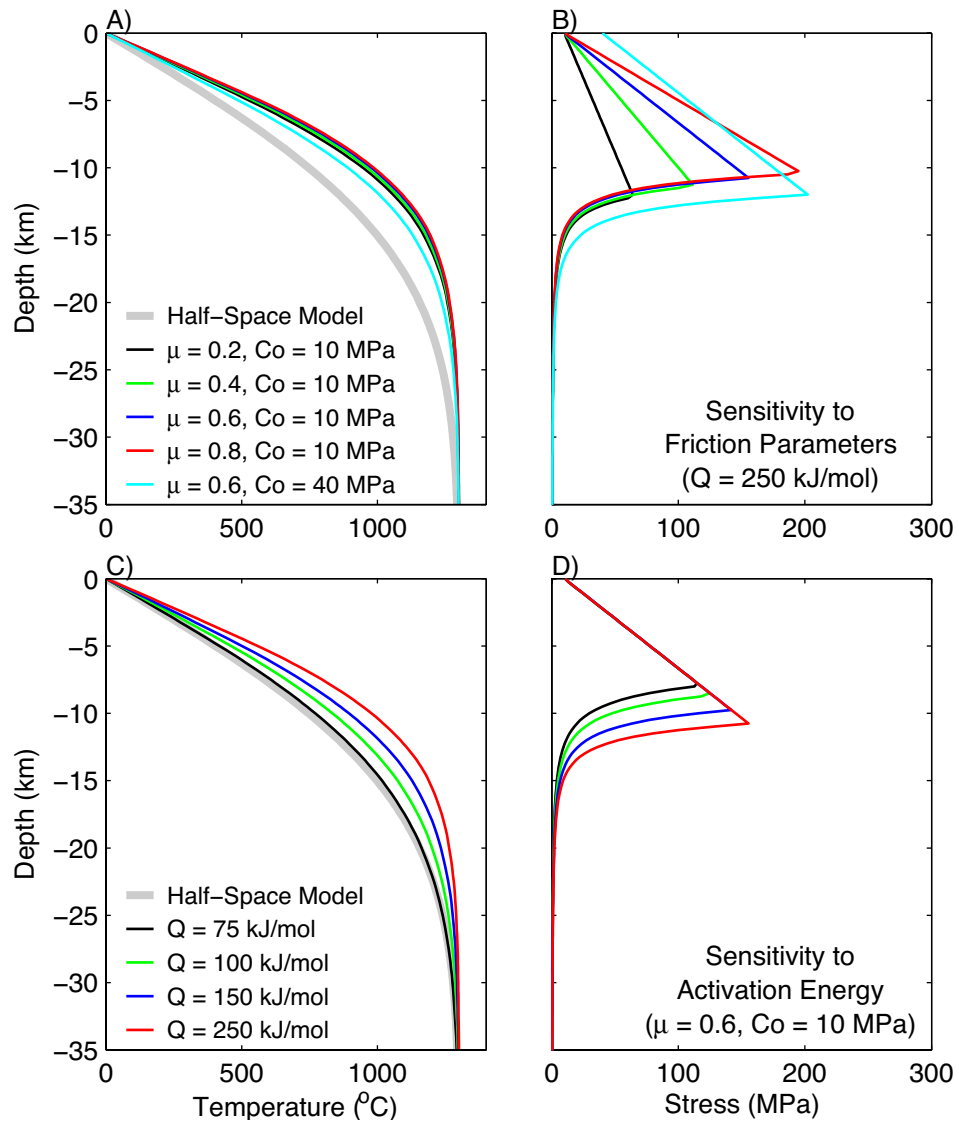


Figure S2

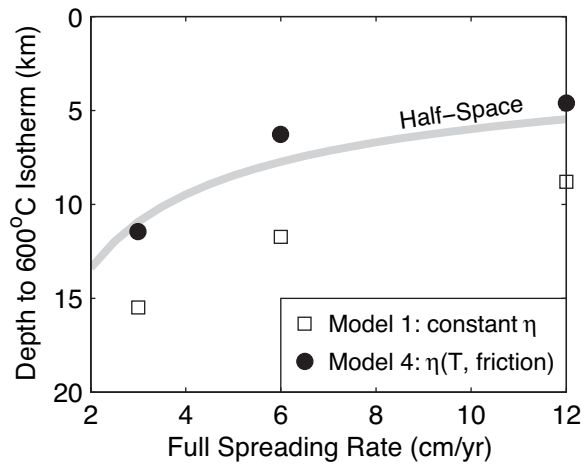


Figure S3